Journal of Applied Physics

Conversion of Shockley partial dislocation pairs from unexpandable to expandable combinations after epitaxial growth of 4H-SiC

Cite as: J. Appl. Phys. **130**, 075107 (2021); https://doi.org/10.1063/5.0047666
Submitted: 16 February 2021 • Accepted: 26 July 2021 • Published Online: 19 August 2021

J. Nishio, C. Ota and R. Iijima

AIP Publishing

Journal of Applied Physics ARTICLE scitation.org/journal/jap

Conversion of Shockley partial dislocation pairs from unexpandable to expandable combinations after epitaxial growth of 4H-SiC

Cite as: J. Appl. Phys. **130**, 075107 (2021); doi: 10.1063/5.0047666
Submitted: 16 February 2021 · Accepted: 26 July 2021 ·
Published Online: 19 August 2021

J. Nishio,[a] C. Ota, and R. Iijima

AFFILIATIONS

Corporate Research and Development Center, Toshiba Corporation, 1 Komukai Toshiba-cho, Saiwai-ku, Kawasaki 212-8582, Japan

[a]**Author to whom correspondence should be addressed:** johji.nishio@toshiba.co.jp

ABSTRACT

Conversion of Shockley partial dislocation pairs from unexpandable to expandable combinations has been considered possible during epitaxial growth. The step-flow model was proposed to explain the conversion, in which an unexpandable 30° C-core partial dislocation in the substrate changes into an expandable 30° Si-core partial dislocation in the epitaxial grown layer. We observed this conversion experimentally by a transmission electron microscope and confirmed the core-species change by high-angle annular dark-field scanning transmission electron microscopy. In addition, other unexpandable combinations of partial dislocations were examined for the possibility of converting to expandable. As a result, the unexpandable basal plane dislocations with a Burgers vector of $\pm(1/3)[11\bar{2}0]$ in the substrate were confirmed to be a necessary condition for forming expandable 30° Si-core partial dislocations after epitaxial growth that could expand single Shockley-type stacking faults and degrade reliability of 4H-SiC power devices.

I. INTRODUCTION

SiC power devices are attracting attention as low-loss devices in the higher blocking-voltage regime in power electronics applications. It is widely accepted that forward voltage degradation in bipolar devices, and even in MOSFETs fabricated on 4H-SiC with *p-n* junctions in the structure, is attributable to the expansion of single Shockley-type stacking fault (1SSF) domains that originate from basal plane dislocations (BPDs).[1–3] The expansion of these domains is explained by migration of Si-core [Si(*g*)] 30° Shockley partial dislocations (PDs)[4] under forward biasing where electron–hole recombination enhances the dislocation glide.[5,6] To resolve the forward degradation, attempts have been made to reduce BPD density by converting BPDs to threading edge dislocations (TEDs) during the epitaxial growth process.[7–13] This helps reduce the number of BPDs that replicate from the substrate to the surface of the epilayer. Another technique is to insert a highly doped buffer layer with a short minority carrier lifetime, and this has successfully suppressed the formation of 1SSF in PiN diodes.[14]

Although 1SSF expansion and contraction phenomena have closely been investigated,[15–24] including using analytical approaches,[25–27] the structure of the PDs that constitute the 1SSF has not yet been fully identified or demonstrated experimentally. Recent microscopic structural analysis studies have made progress in understanding the detailed PD structures.[28–30] These findings are expected to be useful for deciding the criteria for rejecting BPDs by screening.

An analytical investigation of the PD combinations in BPDs noted that combinations of 30° and 90° C-core [C(*g*)] PDs in BPDs are not thought to contribute to 1SSF expansion.[26] We found a 90° C(*g*) PD at the curved line of the BPD in a previous study.[28] Therefore, we assumed that BPDs for which the dislocation lines face the $\pm[\bar{1}2\bar{1}0]$ or $\pm[2\bar{1}\bar{1}0]$ direction have this type of combinations. In another previous study, this type of BPD was found and the structure was confirmed to be a combination of 30° and 90° C (*g*) PDs.[31] In spite of being an unexpandable combination of C(*g*) PDs, the BPDs were the source of triangular 1SSF expansion under forward biasing. It is possible for unexpandable C(*g*) PD to convert into expandable Si(*g*) PD, due to a change in core species while the Burgers vector stays the same as shown in earlier publications.[24–26] This could be realistically possible when the line direction of the PD changes by step-flow motion during epitaxial growth. However, there is no report on experimental evidence concerning the

core-species change directly by structural analysis of the expanded 1SSF, because expandable Si(*g*) PDs that existed as converted PDs before forward biasing moved away.

In this study, to capture the core-species change experimentally, structural analysis was carried out by plan-view transmission electron microscopy (TEM) observation combined with $\boldsymbol{g} \cdot \boldsymbol{b}$ contrast analysis of unexpanded BPDs found in the epilayer. In addition, cross-sectional high-resolution high-angle annular dark-field scanning TEM (HAADF-STEM) imaging was used to determine the core species directly to determine whether expandable Si(*g*) PDs were formed. Moreover, all possible combinations of unexpandable PDs were examined in terms of whether they become expandable or remain unexpandable according to the dislocation-loop model.[24,25] In this way, possible conditions for unexpandable combination of partial dislocations to convert to expandable combination of partial dislocations are revealed.

II. EXPERIMENTAL PROCEDURES

Commercially available *n*-type 4H-SiC (0001) epitaxial wafers with off-cut angles of 4° and 8° in the [11$\bar{2}$0] direction were used. BPDs were detected on the surface of each wafer by photoluminescence (PL) imaging using a Hg-Xe lamp with a 313-nm bandpass filter (BPF) as the excitation source and an excitation power density of about 1.53 W cm^{-2}.[28–30] To observe the 1SSFs bounded by PDs in good contrast, a 420-nm BPF[32] (FWHM: 10 nm) was placed in front of the charged-coupled device detector. Among the detected BPDs, two BPDs among which one had a curved shape were selected for structural analysis. It was actually impossible to select BPDs without any expansion because they had been unintentionally UV-illuminated when examined by PL imaging. Precise locational identification of the PD line end position was confirmed by taking the PL images of the BPDs for the following plan-view TEM imaging. Although the measured length of the [11$\bar{2}$0] line that projected from the longer curved PD could be used to presume the depth where the substrate/epilayer interface was located in each wafer, cross-sectional scanning electron microscopy (SEM) was used for the precise depth determination. Next, samples were thinned by focused ion beam (FIB) milling to analyze the configuration of the PDs, which constitute the BPDs by plan-view bright-field (BF) TEM imaging. In the plan-view TEM analysis, BF images were acquired with the aim of maximizing the dislocation contrast by slight inclination of the sample toward the [11$\bar{2}$0] direction from the [0001] zone axis. In the case of $\boldsymbol{g} \cdot \boldsymbol{b}$ contrast analysis, dark-field images were obtained by a two-beam configuration using three varied diffraction vectors, $\boldsymbol{g}$, of 11$\bar{2}$0, 1$\bar{2}$10, and $\bar{2}$110 at an acceleration voltage of 300 kV.[29,30]

Cross-sectional analysis was then made possible by using the locational information obtained by the plan-view TEM imaging. The appropriate positions for FIB sampling were chosen accordingly. Cross-sectional BF-STEM imaging was carried out to ensure that the 1SSF edges were captured on each BPD. Continuous enlargement by HAADF-STEM enabled high-resolution atomic

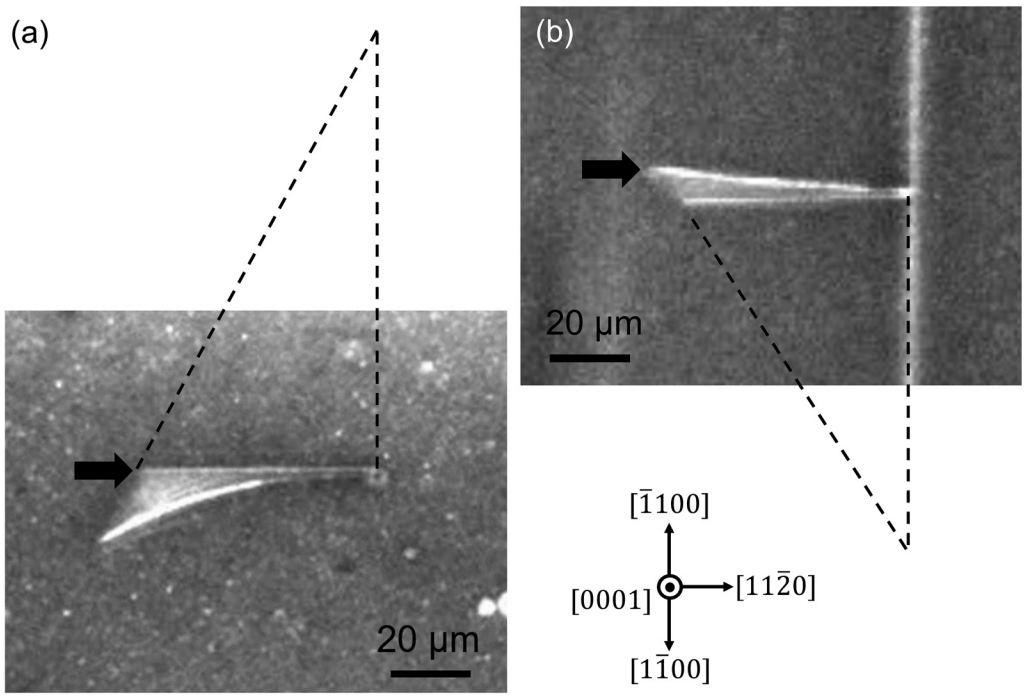

FIG. 1. PL images of the selected BPDs (BPF 420 nm) and expected 1SSF shape when expanded: (a) BPD#1 considered as type A and (b) BPD#2 considered as type B.

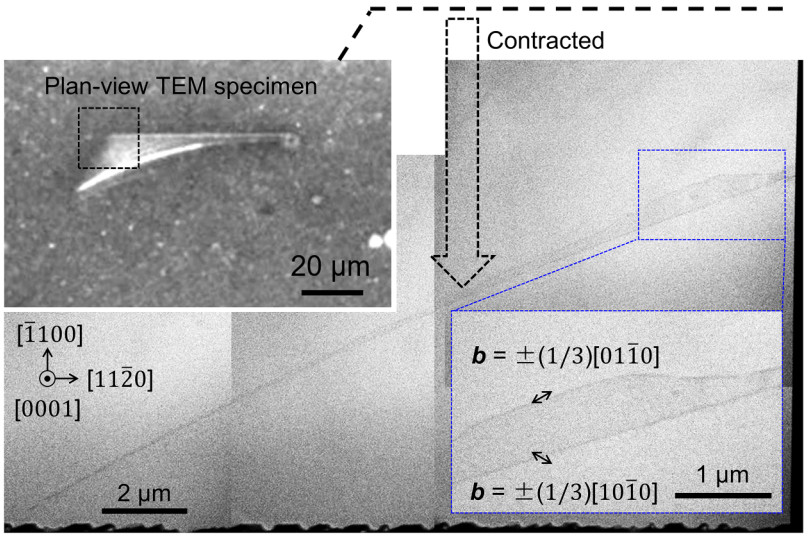

FIG. 2. Plan-view BF-TEM image of BPD#1 and Burgers vectors of PDs derived from the $\boldsymbol{g} \cdot \boldsymbol{b}$ analysis.

imaging for analyzing the PD structures. The HAADF-STEM analyses were carried out at an acceleration voltage of 200 kV.

III. RESULTS AND DISCUSSION

A. Selection of BPDs with unexpandable PDs

Figure 1 shows PL images of the BPDs selected on the different epitaxial wafers. In both images, brighter PL emission in the 1SSF regions between the PDs can be distinguished from the surrounding 4H-SiC. Figure 1(a) shows a BPD with a curved line on the [$1\bar{1}00$] side on the 8° off-cut epitaxial wafer (10.1 μm thick as measured by SEM) without a buffer layer. This BPD is thought to be type A (glide type)[25,26] and is labeled BPD#1. Figure 1(b) shows a BPD with a curved line on the [$\bar{1}100$] side on the 4° off-cut epitaxial wafer (4.9 μm-thick measured by SEM with a 0.5 μm-buffer layer included). This BPD is thought to be type B (glide type)[25,26] and is labeled BPD#2. The difference in off-cut angle is thought to have an influence only on the corresponding depth of the epilayer measured from the lateral length on the straight BPD line observed in the PL images. However, the off-cut angle is expected to make a big difference in step density during epitaxial growth, with the resultant BPD-to-TED conversion ratio higher when the angle is smaller.[10] We treat the effect as negligible in this work because we have confirmed that the difference in the off-cut angle (4° or 8°) in the image force is negligible compared with the effect on the angle with which the dislocation line deviates away from the [11$\bar{2}$0] direction on the basal plane.[33]

Also in Fig. 1, PDs are visible in bright contrast in spite of using the BPF with an FWHM of 10 nm. We think the bright boundaries are due to the tail part of the PL of the PDs with broad peak with an FWHM of ~160 nm and the peak wavelength of about 670–700 nm for Si(g) PD.[28] However, the reason why the left parts of the curved C(g) PDs are brighter than those from the Si(g) PDs is not clear at the moment. Although there is a report that

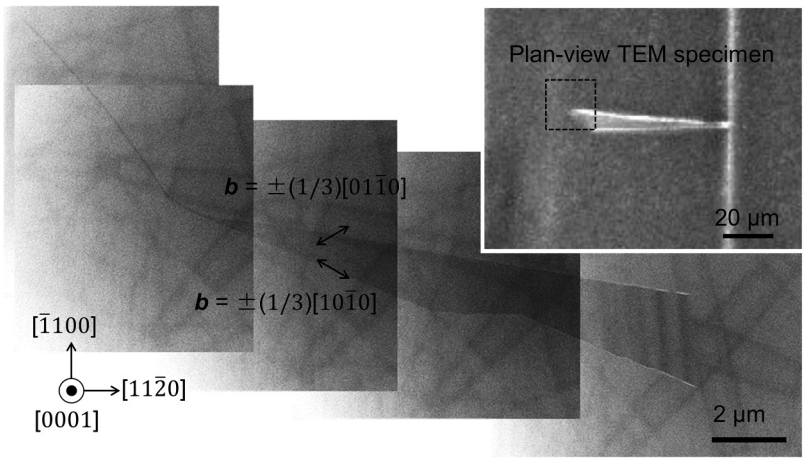

FIG. 3. Plan-view BF-TEM image of BPD#2 and Burgers vectors of PDs derived from the $\boldsymbol{g} \cdot \boldsymbol{b}$ analysis.

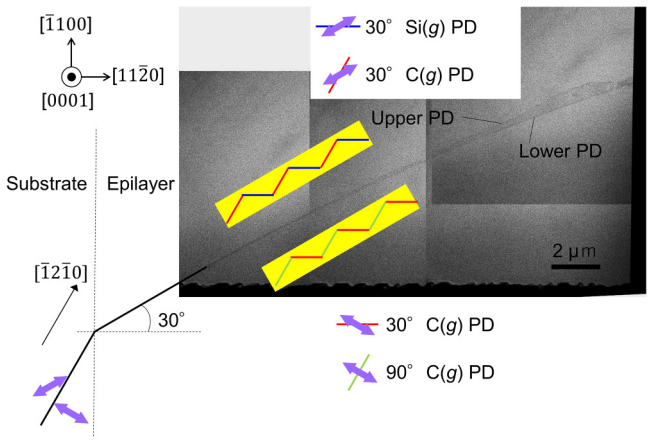

FIG. 4. Speculated shape of BPD#1 in the substrate and interpretation of the dislocation lines observed in the plan-view TEM image.

only 1SSF can be observed in a wavelength range of 450 ± 20 nm,[34] the 4H-SiC background PL emission or PL intensity of the PDs might be different.

Examples of the perfect BPDs replicated from the substrate in an epilayer are shown as transmission x-ray topography images in Ref. 12 and they all have a curved feature more or less. Therefore, curved boundaries shown in Fig. 1 that extend from the substrate/epilayer interface to the top of the epilayer are considered to be the paths of the perfect dislocations. The two 1SSFs shown in Fig. 1 must have developed very rapidly during the initial time of the UV exposure to the shape where the distance between PDs is more than several micrometers, by the movement of Si(*g*) PDs to form straight line along the <11$\bar{2}$0> direction. The distance between unexpanded PDs in the epilayer is reported to be about a few tens of nanometers as they follow Frank's rule to minimize stress energy.[30,35] Therefore, UV illumination should be considered to force Si(*g*)PD to have glided. It should be noted that we have to be careful that the original BPD shapes after the epitaxial growth have been lost when they are observed by PL imaging, especially in case they have Si(*g*) PD as a part. In the PL imaging at near room temperature, only Si(*g*)PD can glide while C(*g*)PD stays still.[36]

B. Plan-view TEM imaging and *g* · *b* contrast analysis

Since the left end of the shorter straight PD indicated by an arrow in Fig. 1(a) is thought to be the deepest part of the leading 30° Si(*g*) PD and the conversion point from the trailing 30° C(*g*) PD, it needed to be included in the plan-view TEM samples. Therefore, the sampling depth was decided so that this part was at the center in the thickness direction of the sample with BPD#1. For in-plane positional determination, a 20 μm square was cut out including the conversion point at the center and the grown-in unexpandable C(*g*) PD. For the sampling of BPD#2, the center in the thickness direction was pointed at the substrate/epilayer interface as indicated by an arrow in Fig. 1(b) in order to observe the dislocation propagating from the substrate to the epilayer. For the in-plane positional determination, a 22 μm square was cut out to center the left end of the grown-in unexpandable curved C(*g*) PD line observed in Fig. 1(b).

The resultant plan-view BF-TEM images for BPD#1 and BPD#2 are shown in Figs. 2 and 3, respectively, with the PL images indicating the sampling positions. Figure 2 shows the lower right part of the square cut-out sample edge. However, the target conversion point from the 30° C(*g*) PD to the 30° Si(*g*) PD does not seem to have been captured within the TEM image. Rather, it seems that the 1SSF area had contracted by movement of the expandable PD close to the unexpandable 30° C(*g*) PD, which was one of a pair of Shockley PDs of BPD#1. The same trend but less serious is seen in Fig. 3 for BPD#2. It has been reported that 1SSF shrinkage is

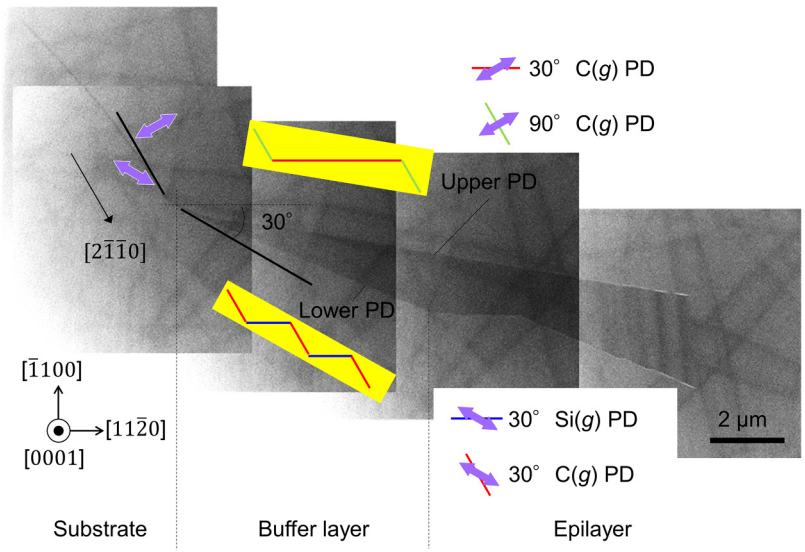

FIG. 5. Interpretation of the dislocation lines observed in the plan-view TEM image of BPD#2.

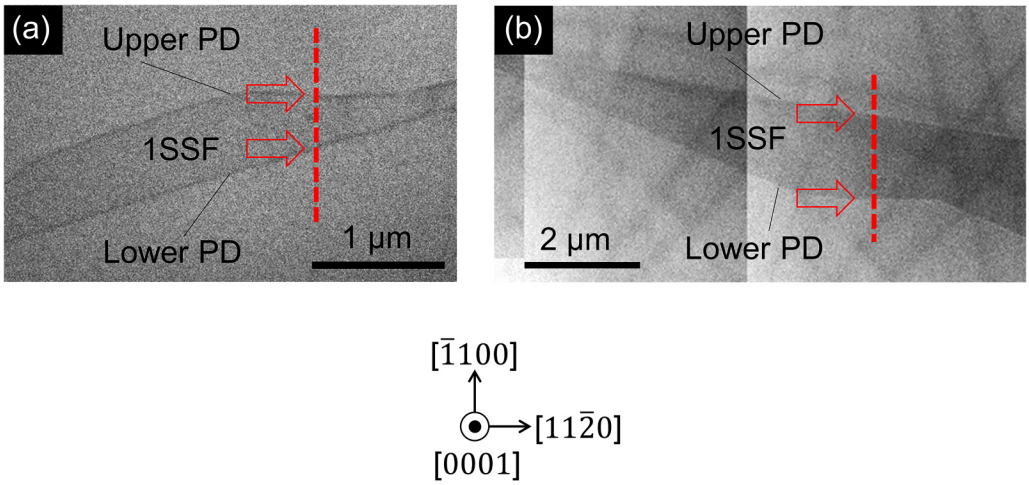

FIG. 6. Cross-sectional HAADF-STEM sampling points and observation direction: (a) BPD#1 and (b) BPD#2.

possible under electron irradiation at RT.[37] Although, quantitative comparison is impossible about what the electron irradiation energy corresponds to electron–hole recombination and/or high temperature,[17,38] the only thing we can speculate to explain this contraction is due to FIB sampling and/or TEM observation. Since the degree of the contraction seems not complete, and the 1SSF contraction was not confirmed during the period of TEM observation, the exact reason why the 1SSF had such long distances between PDs as in

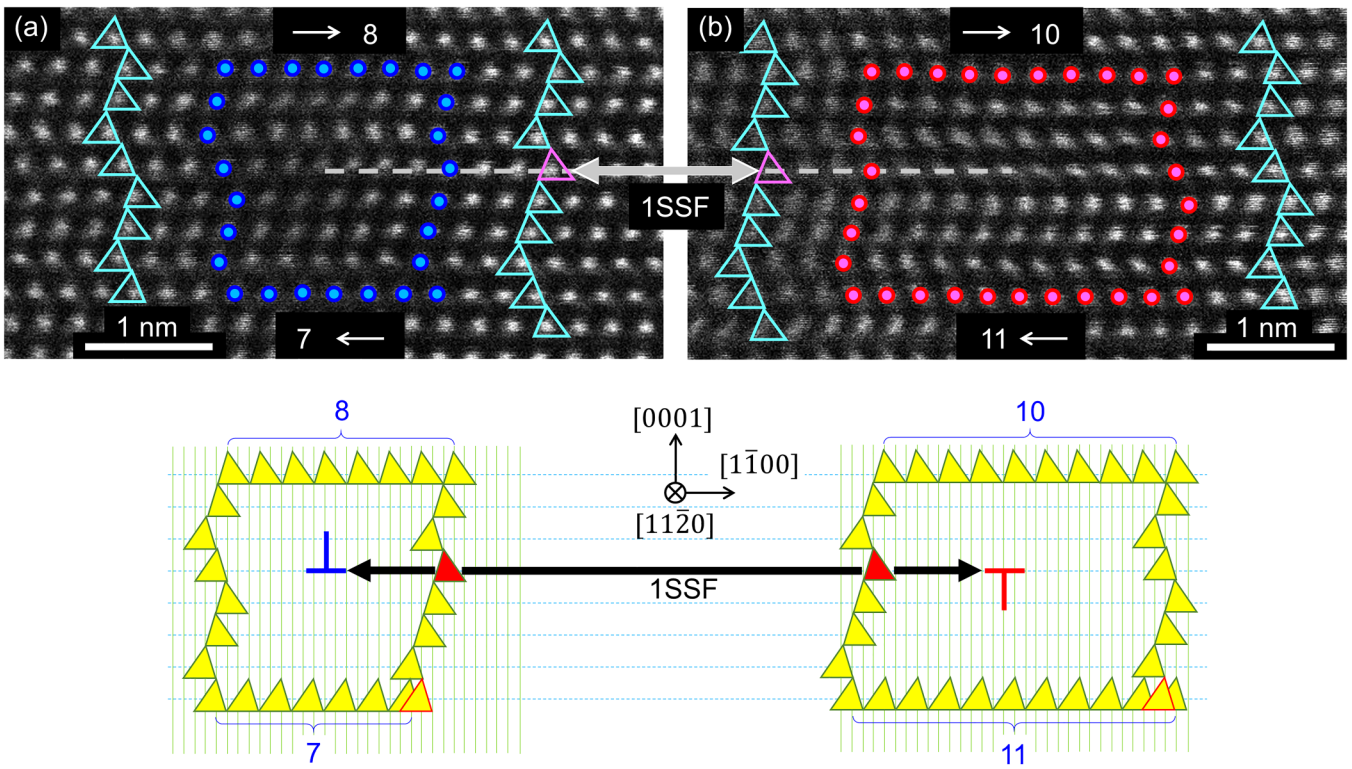

FIG. 7. Cross-sectional HAADF-STEM images, Burgers circuits, and schematic interpretations of PDs of BPD#1: (a) upper PD and (b) lower PD.

Figs. 2 and 3 is unclear at the moment. The shrinkage is due to the Si(g) PD moving back close to where it was after the epitaxial growth, and the C(g) PD not moving. It should be noted that the 1SSF contraction must accompany the glide of a PD, and in the meantime, the line direction changes. However, even the contraction occurred, the immobile C(g) PD propagated in the epilayer should remain where it was after the epitaxial growth, and only the Si(g) containing PD line changes its direction by changing the ratio of constituting PDs. In addition, the vertical relationship of the dislocation contrast in Figs. 2 and 3 is expected to be maintained the same as found in Figs. 1(a) and 1(b), respectively. From Fig. 1(a), the upper and lower lines in Fig. 2 are thought to correspond to 30° Si (g) PD and [30° C(g) + 90° C(g)] PD, respectively.[28] The straight line contrast in the [11$\bar{2}$0] direction in the upper right part of Fig. 2 was enlarged and inset in Fig. 2. Although it became rather short, the residual part of the 30° Si(g) PD parallel to the [11$\bar{2}$0] direction found in Fig. 1(a) can be observed in the inset of Fig. 2.

The left ends of the PD lines in Fig. 2 are in the epilayer, as found in the sampling area for the plan-view TEM specimen. The PD lines are convex and the distance between them is narrower on the left side of Fig. 2. The angle between the PD lines in the left side of Fig. 2 and the [11$\bar{2}$0] direction is 27.7°. This value is close to 30°, where the dislocation line is constructed 50% from 90° C(g) PD in the [$\bar{1}$2$\bar{1}$0] direction and 50% from 30° C(g) PD in the [11$\bar{2}$0] direction. The lines are found to have approached the [11$\bar{2}$0] direction as the epitaxial growth proceeded. This implies that the driving force for the BPD to bend is step-flow. It has been reported previously that PDs are expected to bend toward the step-flow direction during epitaxial growth.[31] According to the current result, the BPD shape in the substrate can be speculated to be as shown in Fig. 4. This speculation contradicts previously published results which conclude that the line of a BPD in the substrate must be parallel or anti-parallel to [11$\bar{2}$0] within 10° to continue into the epilayer as a BPD.[39] This situation can be understood that most BPDs away from this direction had converted to TED under certain epitaxial growth conditions, and the remaining BPDs were observed as penetrated ones close to this direction. In general, BPD-to-TED conversion is strongly dependent on the growth conditions such as C/Si ratio and growth rate. In our cases, the BPD-to-TED conversion mechanism did not seem to function. So, the BPDs that were facing [$\bar{1}$2$\bar{1}$0] as in Fig. 4 or facing [2$\bar{1}\bar{1}$0] as in Fig. 5 are not considered to have been converted to TEDs but to have penetrated into epilayers. By considering the fact in Fig. 3 and in Ref. 31, we think that our current result is not a rare case, and the speculation is not irrelevant. Based on this, the upper and lower dislocation lines in Fig. 4 consist of 30° C(g) and 90° C(g) PDs in the substrate and bend by a combination of 30° C(g) + 30° Si (g) PDs and 90° C(g) + 30° C(g) PDs, respectively, in the epilayer. It is impossible for the upper line to move upward and expand the 1SSF unless it has a Si(g) PD segment in the epilayer. Although the left part of the upper PD line in Fig. 4 is seen as barely bent and

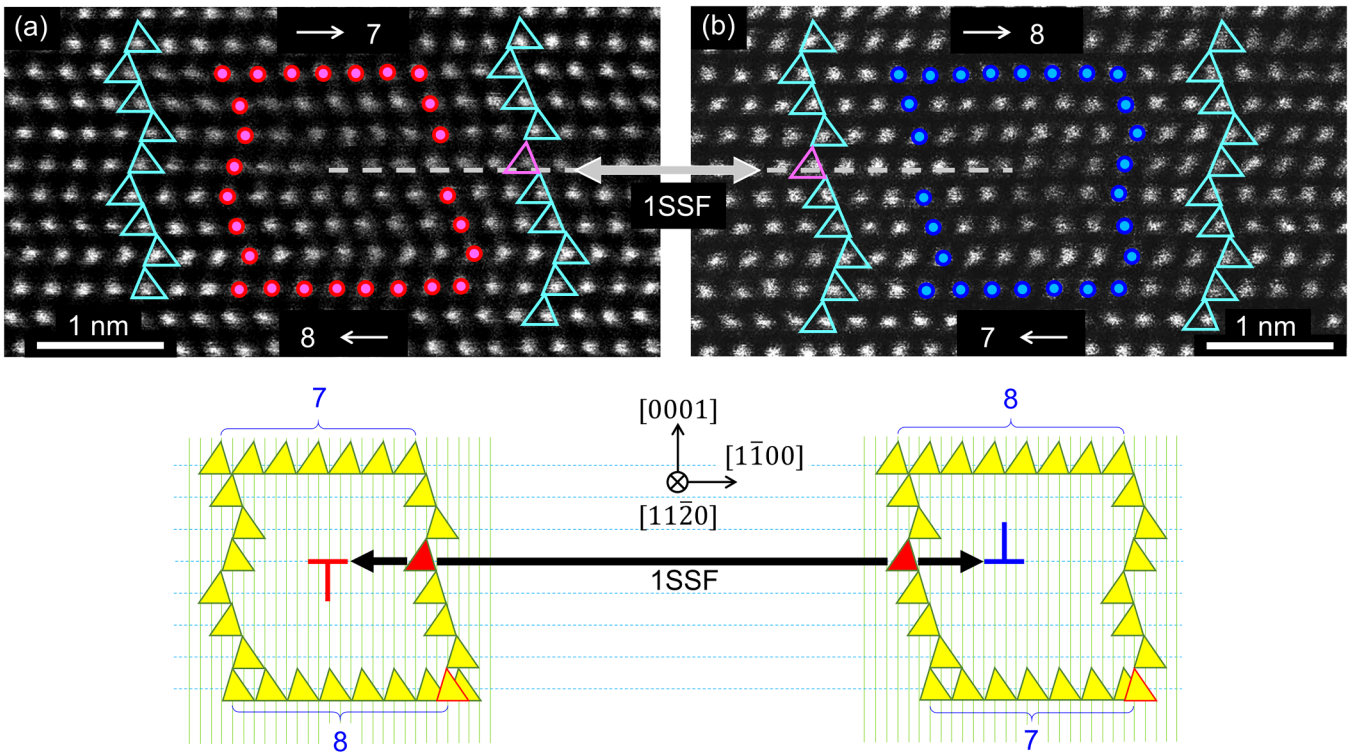

FIG. 8. Cross-sectional HAADF-STEM images, Burgers circuits, and schematic interpretations of PDs of BPD#2: (a) upper PD and (b) lower PD.

containing only 30° C(g) PD, the right end part in Fig. 4 has a short but straight part in the [11$\bar{2}$0] direction, which is considered to be 30° Si(g) PD.

1SSF contraction was also observed in Fig. 3, the same as the result shown in Fig. 2. This made it impossible to detect the target conversion point that was expected at the left end of the straight bright line observed in the PL image shown in Fig. 1(b). Although the 1SSF contracted, it was also observed on BPD#2 that there is a straight parallel line in the [11$\bar{2}$0] direction, which is thought to be a 30° Si(g) PD in Fig. 3. In other words, the upper dislocation line in Fig. 2 and the lower line in Fig. 3 have inflection points that connect to straight lines. At either point in Fig. 2 or 3, the dislocation does not have any contrast implying the presence of TED. Therefore, these inflections are not due to the formation of other dislocation loops accompanying TEDs. It could be that the dislocations only changed their direction while maintaining their own dislocation loops. From Figs. 2 and 3, the dislocation lines are seen to have remained as single continuous lines. This suggests that the Burgers vectors can be expected to be unique to each line. This is confirmed from the results of $\boldsymbol{g}\cdot\boldsymbol{b}$ contrast analysis, in which the entire line contrast disappeared when each extinction rule was satisfied. The Burgers vectors derived from the analysis are also shown in each PD line, namely, for BPD#1, the upper and lower lines in Fig. 2 have ±(1/3)[01$\bar{1}$0] and ±(1/3)[10$\bar{1}$0], respectively, and for BPD#2, the upper and lower lines in Fig. 3 have ±(1/3)[01$\bar{1}$0] and ±(1/3)[10$\bar{1}$0], respectively. Therefore, the composite Burgers vector for BPD#1 and BPD#2 is found to be ±(1/3)[11$\bar{2}$0] in either case when the BPDs are considered to be perfect dislocations. The left end of the PD lines in Fig. 3 is in the substrate, as found in the sampling area for the plan-view TEM specimen. The distance between the PD lines is narrower in the substrate and becomes wider in the epilayer as seen in Fig. 3. Inflection points are also observed in Fig. 3. The positional relationship, such as the substrate/buffer layer interface and buffer layer/epilayer interface, is shown in Fig. 5 based on the sampling information derived from Fig. 1(b). The two inflection points were identified as the above interfaces. The inclination angle of the PD in the buffer layer or epilayer is smaller than that observed in Fig. 4 from the [11$\bar{2}$0] direction. The difference in this angle between BPD#1 and BPD#2 might depend on the growth conditions. Unfortunately, we cannot examine this because the growth conditions are not available for commercial epitaxial wafers. At least, it could be suggested that the degree of step-flow control was stronger in the case of BPD#2. As mentioned before, this might be affected by the difference in off-cut angle. The inflection points observed in Fig. 5 correspond to the location where the growth conditions changed. It is

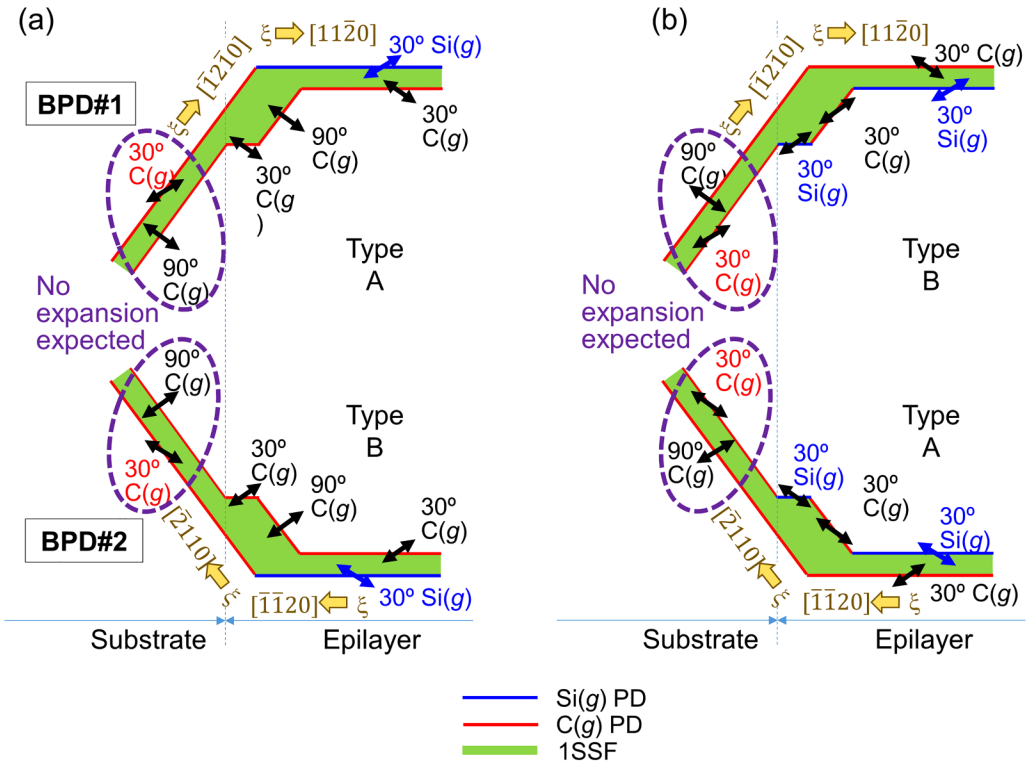

FIG. 9. Possible conversion cases from an unexpandable BPD in the substrate to expandable 30° Si(g) PD in the epilayer: (a) experimentally observed current cases for BPD#1 (type A) and for BPD#2 (type B) and (b) upside down virtual cases of the PD combinations.

reasonable to think that the dominant force driving the dislocation to penetrate perpendicularly to the spiral steps during the sublimation growth changed to propagate perpendicular to the steps of the $(11\bar{2}0)$ face as the epitaxial growth front formed on the surface by the existence of off-cut and bent the direction.[33] The upper PD contrast in Fig. 5 is thought to be a mixture of 90° C(g) and 30° C(g) PDs, the ratio of which varies the angle. An increase in the proportion of 30° C(g) is common in observations of curved BPDs during the progress of the epitaxial growth.[28,31] However, the contrast in the lower PD in Fig. 5 can be due to the mixture of 30° C(g) and 30° Si(g) PDs, the ratio of which can vary the angle, as in the upper PD in Fig. 4. By comparing the angles of the upper PD line in Fig. 4 and the lower PD line in Fig. 5 from the $[11\bar{2}0]$ direction, the portion of 30° Si(g) PD seems larger in BPD#2 than in BPD#1. This does not contradict the result that BPD#2 has a longer straight PD line parallel to the $[11\bar{2}0]$ direction, even within the limited observation area of the TEM images. In a recent report, we selected a 1SSF that expanded in a triangular shape having a baseline arched like a bow as the analysis object and found that the Shockley PDs constituting the BPD in the substrate were an unexpandable combination.[31] It was found from the present study that BPDs with even a small curvature have their direction speculated to be toward $[\bar{1}2\bar{1}0]$ in the case of BPD#1 as in Fig. 4, and experimentally confirmed to be toward $[2\bar{1}\bar{1}0]$ in the case of BPD#2 as in Fig. 5. Whether the PD combinations for these BPDs are unexpandable is investigated below.

C. Cross-sectional HAADF-STEM analysis

It is essential to identify the core species of the PDs and the sign of the Burgers vectors to get a complete picture of whether PDs are converted from unexpandable to expandable combinations or remain unexpandable. The upper and lower PDs in Figs. 4 and 5 were analyzed by cross-sectional HAADF-STEM. The sampling positions were determined to include the straight PD parts observed in the plan-view TEM images as shown in Fig. 6. The FIB sampling positions and directions were decided such that the cross-sectional plane was $(11\bar{2}0)$ perpendicular to the straight PD parts. In both BPD#1 and BPD#2, the upper and lower PD lines were so close that the sample preparation was performed by cutting out single pieces where both PDs were included for both samples as shown by dashed lines in Fig. 6. The HAADF-STEM observation points and direction are also indicated by arrows in Fig. 6. Figure 7 shows the resultant HAADF-STEM images, Burgers circuits, and schematic interpretation of the PDs of BPD#1. The PDs correspond to the 1SSF edges. Si atoms that constitute the Burgers circuit are

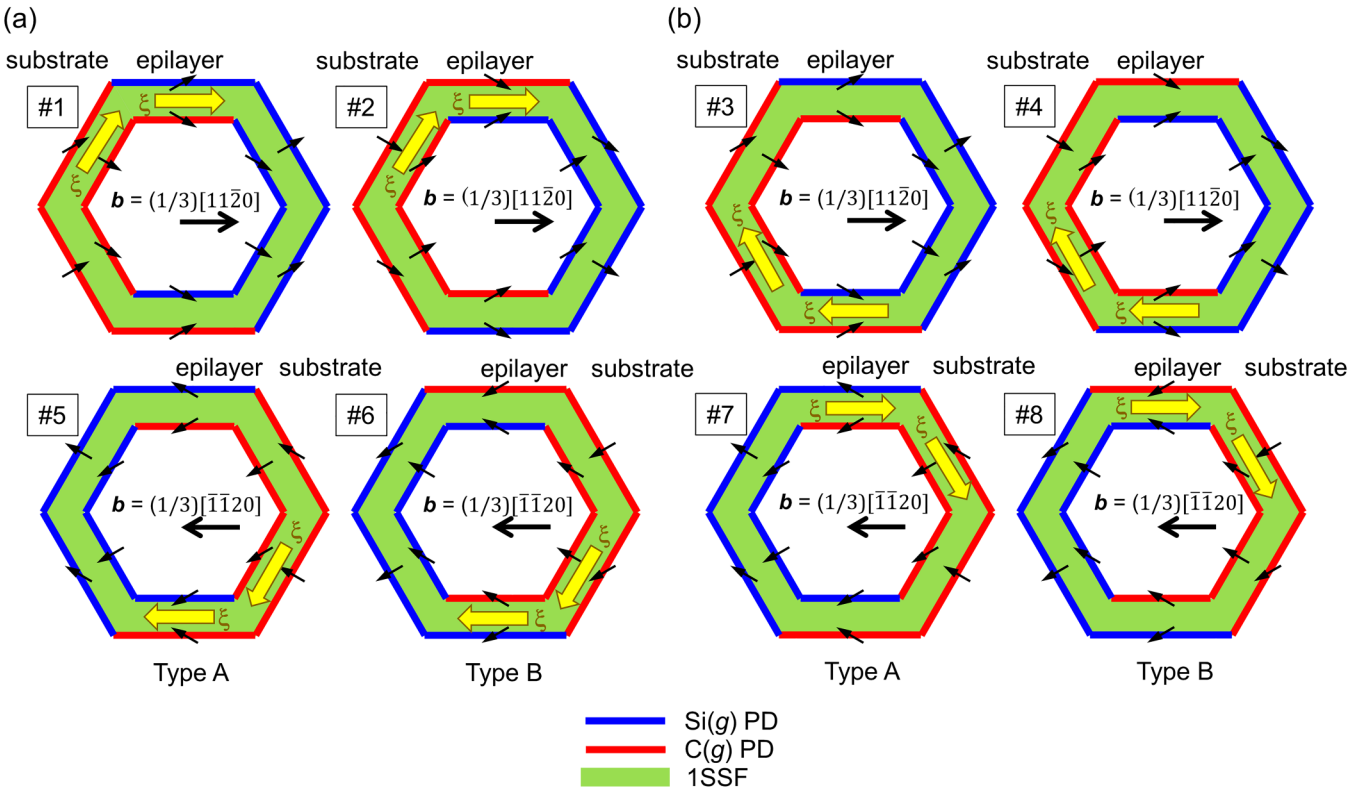

FIG. 10. Conversion from unexpandable BPDs to expandable BPDs represented by dislocation loops and combinations of PDs: (a) dislocation lines of the BPD bending from $\pm[\bar{1}2\bar{1}0]$ to $\pm[11\bar{2}0]$ and (b) bending from $\pm[\bar{2}110]$ to $\pm[\bar{1}\bar{1}20]$.

denoted by circles and tetrahedrons are triangles in Fig. 7. In the Burgers circuit of Fig. 7(a), the number of atoms on the upper side was 8 and on the lower side 7. This indicates that an extra half-plane is inserted on the Si-face side. Additionally, it is seen from Fig. 7(a) that the tetrahedrons are back-to-back on the 1SSF line. These features are characteristic of 30° Si(g).[29] From the FS/RH (perfect) convention combined with the results obtained by $\boldsymbol{g}\cdot\boldsymbol{b}$ contrast analysis (Fig. 2), the Burgers vector for the upper PD of BPD#1 can be uniquely determined[28–31] to be (1/3)[01$\bar{1}$0]. For the lower PD of BPD#1, the number of atoms on the upper side was 10 and on the lower side 11, as seen in Fig. 7(b). This indicates that an extra half-plane is inserted on the C-face side. Additionally, it is seen from Fig. 7(b) that the tetrahedrons are face-to-face on the 1SSF line. These features are characteristic of 30° C(g).[29] From the FS/RH (perfect) convention combined with the results obtained by $\boldsymbol{g}\cdot\boldsymbol{b}$ contrast analysis (Fig. 2), the Burgers vector for the lower PD of BPD#1 can be uniquely determined[28–31] to be (1/3)[10$\bar{1}$0].

In the same manner as in Fig. 7, Fig. 8 shows the resultant cross-sectional HAADF-STEM images, Burgers circuits, and schematic interpretation of the PDs of BPD#2. Si atoms that constitute the Burgers circuit are also denoted by circles and tetrahedrons are triangles in Fig. 8. In the Burgers circuit of Fig. 8(a), the number of atoms on the upper side was 7 and on the lower side 8. This indicates that an extra half-plane is inserted on the C-face side. Additionally, it is seen from Fig. 8(a) that the tetrahedrons are face-to-face on the 1SSF line. These features are characteristic of 30° C(g).[29] From the FS/RH (perfect) convention combined with the results obtained by $\boldsymbol{g}\cdot\boldsymbol{b}$ contrast analysis (Fig. 3), the Burgers vector for the upper PD of BPD#2 can be uniquely determined[28–31] to be (1/3)[0$\bar{1}$10]. For the lower PD of BPD#2, the number of atoms on the upper side was 8 and on the lower side 7, as seen in Fig. 8(b). This indicates that an extra half-plane is inserted on the Si-face side. Additionally, it is seen from Fig. 8(b) that the tetrahedrons are back-to-back on the 1SSF line. These features are characteristic of 30° Si(g).[29] From the FS/RH (perfect) convention combined with the results obtained by $\boldsymbol{g}\cdot\boldsymbol{b}$ contrast analysis (Fig. 3), the Burgers vector for the lower PD of BPD#2 can be uniquely determined[28–31] to be (1/3)[$\bar{1}$010]. From the results obtained above, the composite Burgers vectors for BPD#1 and BPD#2 were determined to be (1/3)[11$\bar{2}$0] and (1/3) [$\bar{1}\bar{1}$20], respectively.

In both cases of BPD#1 and BPD#2, the current results support the model[31] that was proposed experimentally in which expandable 30° Si(g) can be formed in the epilayer by conversion of unexpandable 30° C(g) in the substrate. This also indicates that the model is valid for the distinction of BPDs by the structure of the nearest layers above and below the slip plane as described either type A or type B in the dislocation loop model.[25,27]

TABLE I. Summary of the conversion cases from unexpandable BPDs to expandable BPDs with Burgers vectors, directions of BPDs, constituent PDs, corresponding fully expanded triangular 1SSF shapes, and glide types.

No.	$\boldsymbol{b}_{BPD}$	ξ_{BPD}	$\boldsymbol{b}_{PD\ (immobile\ in\ substrate)}$	$\boldsymbol{b}_{PD\ (in\ epilayer)}$	1SSF shape	Glide type
1	(1/3)[11$\bar{2}$0]	[$\bar{1}$2$\bar{1}$0]	30°C-core [01$\bar{1}$0] 90°C-core [10$\bar{1}$0]	30°Si-core [01$\bar{1}$0] 30°C-core [10$\bar{1}$0]		Type A **(BPD#1)**
2			90°C-core [10$\bar{1}$0] 30°C-core [01$\bar{1}$0]	30°C-core [10$\bar{1}$0] 30°Si-core [01$\bar{1}$0]		Type B
3		[$\bar{2}$110]	30°C-core [101$\bar{0}$] 90°C-core [011$\bar{0}$]	30°Si-core [101$\bar{0}$] 30°C-core [011$\bar{0}$]		Type A
4			90°C-core [011$\bar{0}$] 30°C-core [101$\bar{0}$]	30°C-core [011$\bar{0}$] 30°Si-core [101$\bar{0}$]		Type B
5	(1/3)[$\bar{1}\bar{1}$20]	[1$\bar{2}$10]	30°C-core [0$\bar{1}$10] 90°C-core [$\bar{1}$010]	30°Si-core [0$\bar{1}$10] 30°C-core [$\bar{1}$010]		Type A
6			90°C-core [$\bar{1}$010] 30°C-core [0$\bar{1}$10]	30°C-core [$\bar{1}$010] 30°Si-core [0$\bar{1}$10]		Type B
7		[2$\bar{1}\bar{1}$0]	30°C-core [$\bar{1}$010] 90°C-core [0$\bar{1}$10]	30°Si-core [$\bar{1}$010] 30°C-core [0$\bar{1}$10]		Type A
8			90°C-core [0$\bar{1}$10] 30°C-core [$\bar{1}$010]	30°C-core [0$\bar{1}$10] 30°Si-core [$\bar{1}$010]		Type B **(BPD#2)**

D. Conditions for conversion from unexpandable BPDs to expandable combinations of PDs

From the current examination, the cases of conversion from unexpandable BPDs to expandable combinations of PDs which possess expandable 30° Si(g) PDs are shown schematically in Fig. 9. Figure 9(a) shows the experimentally confirmed cases and Fig. 9(b) shows virtual cases for the PD combinations upside down from Fig. 9(a). In Fig. 9(a), the change in PD combination in the substrate and the epilayer is illustrated for BPD#1 and BPD#2 as type A and type B, respectively. The conversion from unexpandable BPDs to expandable combinations of the PDs is possible only when the Burgers vector of the BPD, $\boldsymbol{b}_{\mathrm{BPD}}$, is (1/3)[11$\bar{2}$0] or (1/3)[$\bar{1}\bar{1}$20] and their dislocation direction, ξ_{BPD}, is bent from [$\bar{1}$2$\bar{1}$0] to [11$\bar{2}$0] (the upper pictures in Fig. 9) or from [$\bar{2}$110] to [$\bar{1}\bar{1}$20] (the lower pictures in Fig. 9).[31] In any case, BPDs in the substrate surrounded by dashed ellipses in Fig. 9 have unexpandable combinations of PDs. The arrows in both directions denote the two possible directions. In these four cases, when the 1SSF expands fully toward the surface of the epilayer by UV illumination or forward biasing, its shape is expected to be triangular and have a right-angled corner at the surface side of the epilayer, as shown by dashed lines in Fig. 1.

Next, when we consider the virtual cases where the PDs are turned upside-down as in Fig. 9(b), and the relationship between type A and type B becomes the opposite. As can be expected from Burgers vector direction of expandable 30° Si(g) PD, the expansion direction is toward the substrate/epilayer interface. Therefore, converted BPDs having 30° Si(g) PDs that penetrated through the epilayer close to the surface are expected to form triangular 1SSFs having a right-angled corner at the substrate side when expanded fully. As derived from Fig. 9(a), the expected 1SSF shape is the same independent of the $\boldsymbol{b}_{\mathrm{BPD}}$ sign, i.e., (1/3)[11$\bar{2}$0] or (1/3)[$\bar{1}\bar{1}$20].

In order to check if every case is covered by the conditions for conversion from unexpandable BPDs to expandable combinations of PDs, the dislocation loop model[25] is employed, which is based on the preceding idea that BPDs are expected to have cores comprising two extra half-planes.[24] Figure 10 shows the conversion from unexpandable BPDs to expandable BPDs represented by the dislocation loops and combinations of PDs. The ways in which dislocation lines of the BPDs, ξ_{BPD}, bend from ±[$\bar{1}$2$\bar{1}$0] in the substrate to ±[11$\bar{2}$0] in the epilayer and bend from ±[$\bar{2}$110] to ±[$\bar{1}\bar{1}$20] are shown on the dislocation loops in Figs. 10(a) and 10(b), respectively. There are no possible cases other than the eight cases shown

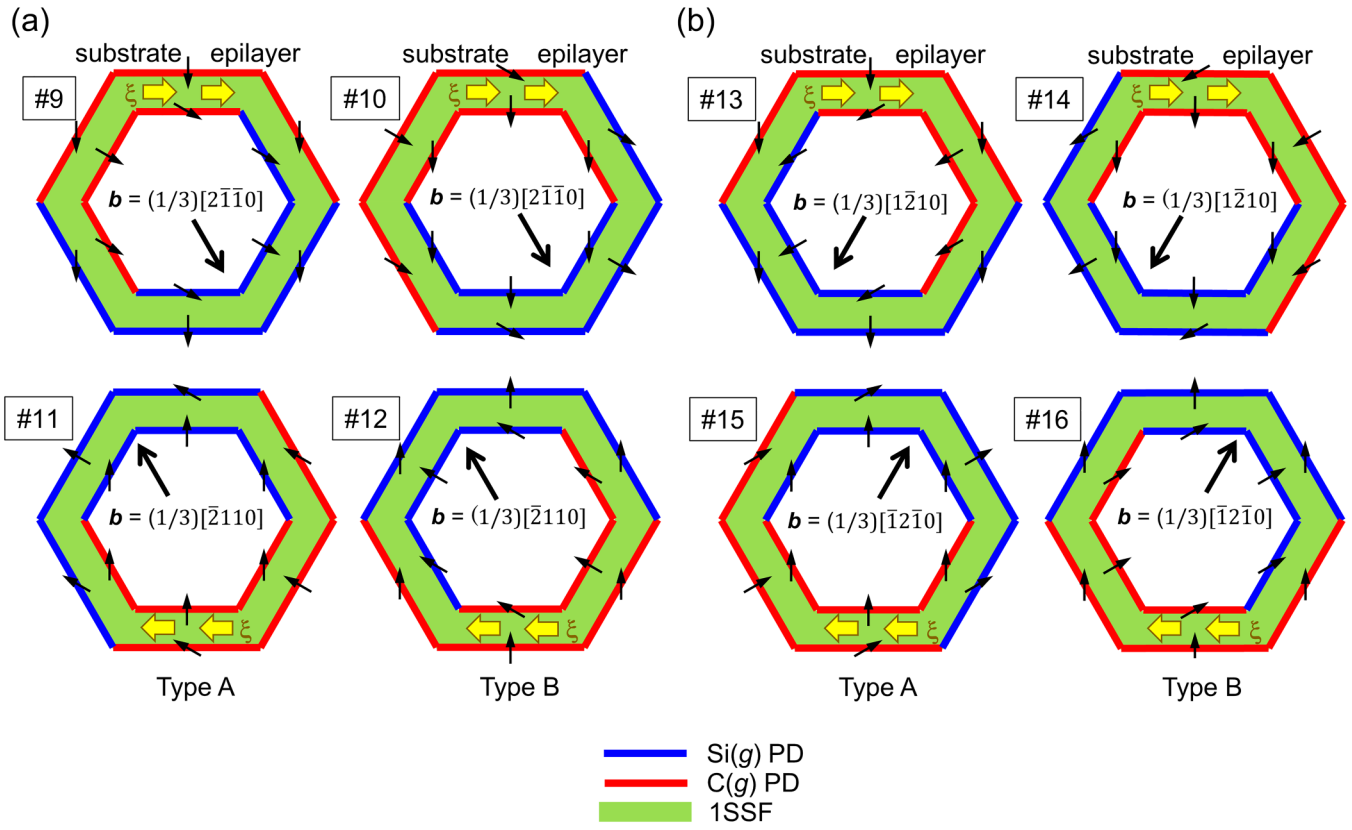

FIG. 11. Possibilities of case 1, where the unexpandable BPDs in the substrate replicate to the epilayer without changing character, represented by dislocation loops and combinations of PDs: (a) ξ_{BPD} is ±[11$\bar{2}$0] and $\boldsymbol{b}_{\mathrm{BPD}}$ is ±(1/3)[2$\bar{1}\bar{1}$0] and (b) ξ_{BPD} is ±[11$\bar{2}$0] and $\boldsymbol{b}_{\mathrm{BPD}}$ is ±(1/3)[$\bar{1}$2$\bar{1}$0].

in Fig. 10 because unexpandable combinations consist of 30° C(g) and 90° C(g), and at least one of the converted PDs is 30° Si(g). These eight cases are summarized in Table I. From Table I, the necessary condition for the unexpandable BPDs to have unexpandable PD combinations of 30° C(g) and 90° C(g) and vice versa in a substrate that is bent toward the step flow direction of $[11\bar{2}0]$ in the epilayer and for the 30° C(g) PD to change to expandable 30° Si(g) is limited to only when $\boldsymbol{b}_{\mathrm{BPD}} = \pm(1/3)[11\bar{2}0]$. From the structural analysis results of BPD#1 and BPD#2, these can be assigned to cases #1 and #8, respectively, in Fig. 10 and Table I. As far as we know, the expanded 1SSF shape with right-angled corner at the substrate side as in the cases of #2, #3, #6, and #7 (pink triangles in Table I) have never been appeared from BPDs in which one of the pair of PDs had a curved shape, so far. In other words, there are no reports of observation of the 1SSF expansion of type B character where the original BPDs were $\xi_{\mathrm{BPD}} = \pm[\bar{1}2\bar{1}0]$ in the substrate and bent to the $\pm[11\bar{2}0]$ direction in the epilayer, or 1SSF expansion of type A character where the original BPDs were $\xi_{\mathrm{BPD}} = \pm[\bar{2}110]$ in the substrate and bent to the $\pm[\bar{1}\bar{1}20]$ direction in the epilayer. Statistically, the glide type of the BPD (type A or B) is expected to be fifty-fifty.

E. Conditions for unexpandable BPDs remaining unexpandable

There are cases where BPDs in the substrate having unexpandable combinations of PDs may replicate without changing direction, and thus the PDs remain unexpandable (we refer to this cases as case 1). There are cases where the BPDs bend from the $\pm[\bar{1}2\bar{1}0]$ or $\pm[\bar{2}110]$ direction in the substrate to the $\pm[11\bar{2}0]$ or $\pm[\bar{1}\bar{1}20]$ direction in the epilayer, respectively, and the PDs are converted to combinations that remain unexpandable (we refer to this as case 2). In order to check all cases, the dislocation loop model[25] is employed again.

In case 1, the BPDs where ξ_{BPD} is $[11\bar{2}0]$ or $[\bar{1}\bar{1}20]$ in the substrate replicate to the epilayer without bending. The number of combinations found was 8 by verification using the dislocation loop model as shown in Fig. 11. In the cases where ξ_{BPD} is $\pm[11\bar{2}0]$, the corresponding $\boldsymbol{b}_{\mathrm{BPD}}$ is $(1/3)[2\bar{1}\bar{1}0]$ or $(1/3)[\bar{2}110]$ as shown in Fig. 11(a), or $(1/3)[\bar{1}2\bar{1}0]$ or $(1/3)[\bar{1}\bar{1}20]$ as shown in Fig. 11(b). In every case, since ξ_{BPD} is parallel to the step flow direction, it is most energetically favorable for the BPDs to replicate by maintaining their direction without being affected by the bending force.[33]

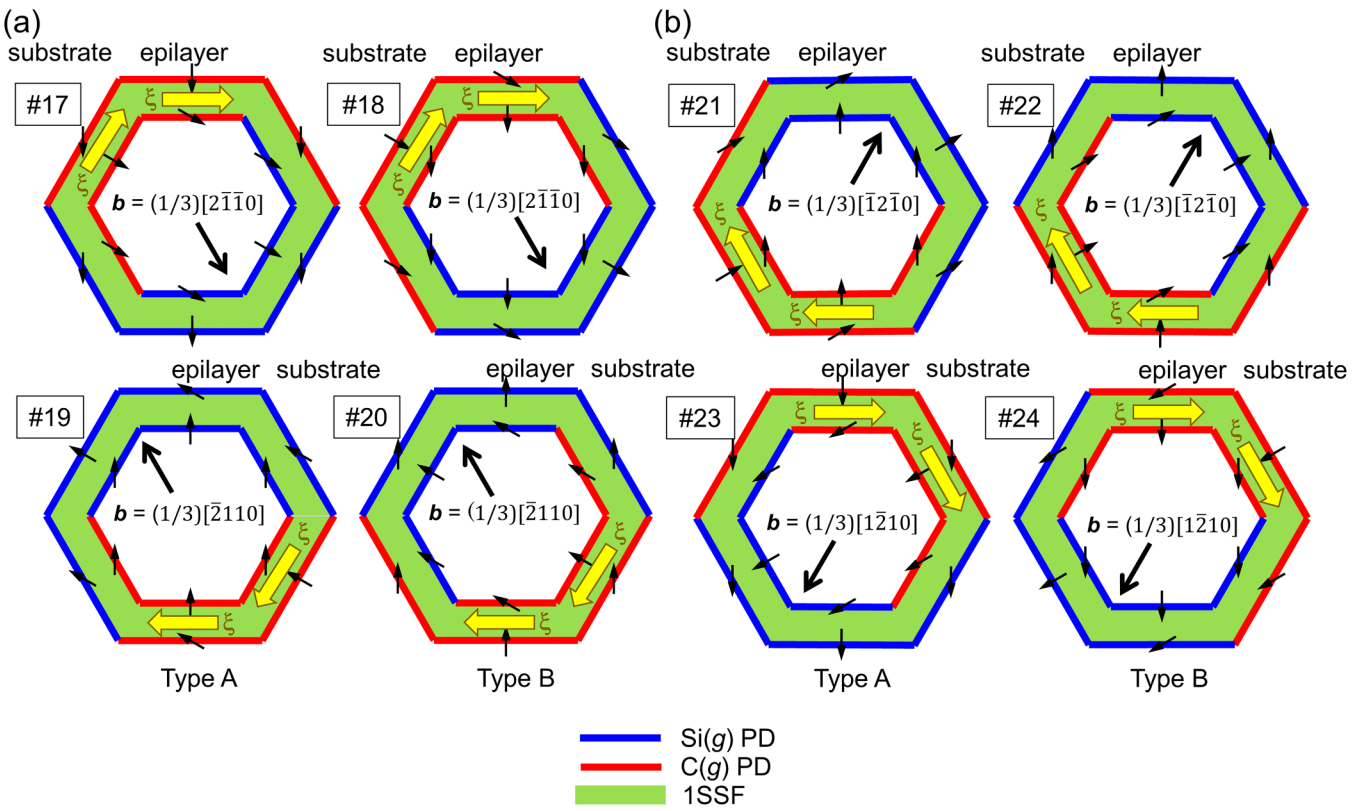

FIG. 12. Possibilities of case 2, conversion from unexpandable BPDs to other unexpandable BPDs represented by dislocation loops and combinations of PDs: (a) dislocation lines of the BPD bending from $\pm[\bar{1}2\bar{1}0]$ to $\pm[11\bar{2}0]$ and (b) bending from $\pm[\bar{2}110]$ to $\pm[\bar{1}\bar{1}20]$.

In case 2, the number of combinations found was 8 by verification using the dislocation loop model as shown in Fig. 12. Figure 12 shows the conversion from unexpandable BPDs to other unexpandable BPDs represented by the dislocation loops and the combinations of PDs. The ways in which the dislocation lines of the BPDs, ξ_{BPD}, bent from $\pm[\bar{1}2\bar{1}0]$ in the substrate to $\pm[11\bar{2}0]$ in the epilayer and from $\pm[\bar{2}110]$ to$\pm[\bar{1}\bar{1}20]$ are shown on the dislocation loops in Figs. 12(a) and 12(b), respectively. The corresponding $\boldsymbol{b}_{BPD}$ are $\pm(1/3)[2\bar{1}\bar{1}0]$ and $\pm(1/3)[\bar{1}2\bar{1}0]$ for the cases in Figs. 12(a) and 12(b), respectively. In all of the cases in Fig. 12, even though the PDs are converted by bending the BPD, the conversion is from non-expandable PD combinations of 30° C(g) and 90° C(g) to also non-expandable combinations of 90° C(g) and 30° C(g), or vice versa. Accordingly, the number of combinations where BPDs in the substrate remained unexpandable into the epilayer combined with case 1 and case 2 is found to be 16.

IV. CONCLUSIONS

We performed a detailed analysis of the structure of unexpanded BPDs to confirm the validity of a previously proposed model in which BPDs in the substrate having unexpandable combinations of 90° C(g) and 30° C(g) PDs may change their direction by the epitaxial step flow and 30° C(g) PD is converted to an expandable 30° Si(g) PD in the epilayer. With the aid of plan-view TEM imaging, and the following cross-sectional HAADF-STEM imaging, the core-species change from C(g) in the substrate to Si (g) in epilayer has been confirmed experimentally. Other possible conditions for conversion from 30° C(g) to 30° Si(g) PD were examined based on the dislocation loop model. The conditions where the unexpandable BPDs in the substrate remain unexpandable even by replicating or changing to other unexpandable combinations were also examined.

DATA AVAILABILITY

The data that support the findings of this study are available within the article.

REFERENCES

[1]J. Q. Liu, M. Skowronski, C. Hallin, R. Söderholm, and H. Lendenmann, Appl. Phys. Lett. **80**, 749 (2002).
[2]P. O. Å. Persson, L. Hultman, H. Jacobson, J. P. Bergman, E. Janzén, J. M. Molina-Aldareguia, W. J. Clegg, and T. Tuomi, Appl. Phys. Lett. **80**, 4852 (2002).
[3]M. Skowronski and S. Ha, J. Appl. Phys. **99**, 011101 (2006).
[4]S. Ha, M. Benamara, M. Skowronski, and H. Lendenmann, Appl. Phys. Lett. **83**, 4957 (2003).
[5]J. D. Weeks, J. C. Tully, and L. C. Kimerling, Phys. Rev. B **12**, 3286 (1975).
[6]K. Maeda and S. Takeuchi, in *Dislocations in Solids*, edited by F. R. N. Nabarro and M. S. Duesbery (North-Holland, Amsterdam, 1996), Vol. 10, pp. 435–504.
[7]H. Jacobson, J. Birch, R. Yakimova, M. Syväjärvi, J. P. Bergman, A. Ellison, T. Tuomi, and E. Janzén, J. Appl. Phys. **91**, 6354 (2002).
[8]S. Ha, P. Mieszkowski, M. Skowronski, and L. B. Rowland, J. Cryst. Growth **244**, 257 (2002).
[9]T. Ohno, H. Yamaguchi, S. Kuroda, K. Kojima, T. Suzuki, and K. Arai, J. Cryst. Growth **260**, 209 (2004).
[10]W. Chen and M. A. Capano, J. Appl. Phys. **98**, 114907 (2005).
[11]Z. Zhang and T. S. Sudarshan, Appl. Phys. Lett. **87**, 151913 (2005).
[12]H. Tsuchida, M. Ito, I. Kamata, and M. Nagano, Phys. Status Solidi B **246**, 1553 (2009).
[13]R. E. Stahlbush, B. L. VanMil, R. L. Myers-Ward, K.-K. Lew, D. K. Gaskill, and C. R. Eddy, Appl. Phys. Lett. **94**, 041916 (2009).
[14]T. Tawara, T. Miyazawa, M. Ryo, M. Miyazato, T. Fujimoto, K. Takenaka, S. Matsunaga, M. Miyajima, A. Otsuki, Y. Yonezawa, T. Kato, H. Okumura, T. Kimoto, and H. Tsuchida, J. Appl. Phys. **120**, 115101 (2016).
[15]T. Miyanagi, H. Tsuchida, I. Kamata, and T. Nakamura, Appl. Phys. Lett. **89**, 062104 (2006).
[16]J. D. Caldwell, R. E. Stahlbush, K. D. Hobart, O. J. Glembocki, and K. X. Liu, Appl. Phys. Lett. **90**, 143519 (2007).
[17]J. D. Caldwell, R. E. Stahlbush, M. G. Ancona, O. J. Glembocki, and K. D. Hobart, J. Appl. Phys. **108**, 044503 (2010).
[18]Y. Iwahashi, M. Miyazato, M. Miyajima, Y. Yonezawa, T. Kato, H. Fujiwara, K. Hamada, A. Otsuki, and H. Okumura, Mater. Sci. Forum **897**, 218 (2017).
[19]S. Hayashi, T. Yamashita, J. Senzaki, M. Miyazato, M. Ryo, M. Miyajima, T. Kato, Y. Yonezawa, K. Kojima, and H. Okumura, Jpn. J. Appl. Phys. **57**, 04FR07 (2018).
[20]A. Okada, J. Nishio, R. Iijima, C. Ota, A. Goryu, M. Miyazato, M. Ryo, T. Shinohe, M. Miyajima, T. Kato, Y. Yonezawa, and H. Okumura, Jpn. J. Appl. Phys. **57**, 061301 (2018).
[21]T. Tanaka, H. Shiomi, N. Kawabata, Y. Yonezawa, T. Kato, and H. Okumura, Appl. Phys. Express **12**, 041006 (2019).
[22]A. Okada, C. Ota, J. Nishio, A. Goryu, R. Iijima, K. Nakayama, T. Kato, Y. Yonezawa, and H. Okumura, Mater. Sci. Forum **963**, 280 (2019).
[23]A. Iijima and T. Kimoto, Appl. Phys. Lett. **116**, 092105 (2020).
[24]N. Zhang, Y. Chen, Y. Zhang, M. Dudley, and R. E. Stahlbush, Appl. Phys. Lett. **94**, 122108 (2009).
[25]H. Matsuhata, H. Yamaguchi, T. Yamashita, T. Tanaka, B. Chen, and T. Sekiguchi, Philos. Mag. **94**, 1674 (2014).
[26]A. Iijima, I. Kamata, H. Tsuchida, J. Suda, and T. Kimoto, Philos. Mag. **97**, 2736 (2017).
[27]H. Matsuhata and T. Sekiguchi, Philos. Mag. **98**, 878 (2018).
[28]J. Nishio, A. Okada, C. Ota, and M. Kushibe, Mater. Sci. Forum **1004**, 376 (2020).
[29]J. Nishio, A. Okada, C. Ota, and M. Kushibe, J. Electron. Mater. **49**, 5232 (2020).
[30]J. Nishio, A. Okada, C. Ota, and R. Iijima, J. Appl. Phys. **128**, 085705 (2020).
[31]J. Nishio, A. Okada, C. Ota, and R. Iijima, Jpn. J. Appl. Phys. **60**, SBBD01 (2021).
[32]S. G. Sridhara, F. H. C. Carlsson, J. P. Bergman, and E. Janzén, Appl. Phys. Lett. **79**, 3944 (2001).
[33]J. Nishio, C. Ota, A. Okada, and R. Iijima, Phys. Status Solidi A **217**, 2000332 (2020).
[34]A. Galeckas, J. Linnros, and P. Pirouz, Appl. Phys. Lett. **81**, 883 (2002).
[35]X. Zhang, M. Nagano, and H. Tsuchida, Mater. Sci. Forum **717–720**, 335 (2012).
[36]M. H. Hong, A. V. Samant, and P. Pirouz, Philos. Mag. A **80**, 919 (2000).
[37]Y. Ohno, I. Yonenaga, K. Miyao, K. Maeda, and H. Tsuchida, Appl. Phys. Lett. **101**, 042102 (2012).
[38]A. Iijima and T. Kimoto, J. Appl. Phys. **126**, 105703 (2019).
[39]Z. Zhang and T. S. Sudarshan, Appl. Phys. Lett. **87**, 161917 (2005).